JOURNAL OF GEOPHYSICAL RESEARCH, VOL. 111, C12025, doi:10.1029/2006JC003565, 2006

Middepth equatorial tracer tongues in a model of the Atlantic Ocean

Carsten Eden[1]

Received 22 February 2006; revised 8 August 2006; accepted 25 August 2006; published 28 December 2006.

[1] Observational estimates of middepth tracer tongues in the equatorial Atlantic are reviewed and are compared with results from several eddy-resolving model simulations. Local maxima of chlorofluorocarbon (CFC) concentrations along the equator at around 1500 m depth are related to mean eastward jet structures in the models at similar depth ranges and can also be identified in several simulated tracer distributions. Similar to the observations, strong eastward jets are located in the simulations 1°–2° north and south of the equator. The model simulations show, in addition, consistent with the CFC observations, weaker jets at around 4°–6°N/S and 8°–10°N/S, suggestive of a large-scale alternating eastward/westward current system in the western tropical Atlantic in this depth range. Lagrangian transport estimates in the model using float diagnostics show a transport of 1–3 Sv in each of the eastward jets 1°–2°N/S off the equator compared to 3–12 Sv throughflow into the South Atlantic, with no seasonal cycle apparent in the transport fractioning. Comparing different model solutions reveals the choice of the subgrid-scale mixing parameterization as important for the amplitudes of the jets. Enhanced (reduced) diapycnal mixing is related to stronger (weaker) jets.

Citation: Eden, C. (2006), Middepth equatorial tracer tongues in a model of the Atlantic Ocean, *J. Geophys. Res.*, *111*, C12025, doi:10.1029/2006JC003565.

1. Introduction

[2] A series of recent direct current observations has revealed rather strong, i.e., up to 10 cm/s, and complex zonal current structures in the middepth equatorial Atlantic [*Schott et al.*, 2003] with a large annual cycle superimposed [*Jochum and Malanotte-Rizzoli*, 2003; *Brandt and Eden*, 2004]. Although similar flow structures can be found in the other equatorial ocean basins as well, the equatorial Atlantic is of special interest, since here, the lower part of the meridional overturning circulation has to pass this complex and fluctuating zonal flow regime. During the passage of the deep meridional flow, its water mass characteristics, which are otherwise more or less conserved in the interior, higher-latitude ocean, might be altered because of lateral or vertical mixing in the energetic zonal flow regimes near the equator [*Lux et al.*, 2001; *Schott et al.*, 2003]. Furthermore, it has been speculated [*Johnson and Marshall*, 2002] that southward spreading transient tracer signals or dynamical wave-like processes imprinted further upstream, might be delayed or even stopped because of possible zonal excursions along the equator of the deep southward flow.

[3] Such zonal excursion of transient signals have indeed been reported for chlorofluorocarbon (CFC) measurements, [e.g., *Weiss et al.*, 1985; *Rhein et al.*, 1995; *Outdot et al.*, 1998; *Andrie et al.*, 1998]. Since the beginning of the 1980 to 1990, CFC concentrations are detectable and increasing in the deep western boundary current (DWBC) of the tropical North Atlantic but stay very low above in the intermediate water masses and in the surrounding water of the DWBC. However, in a depth range of 1000 to 2000 m, CFC maxima have been found along the equator also in the interior with decaying amplitudes to the east, pointing toward eastward zonal transports, connecting the DWBC with the interior equatorial Atlantic. While early CFC measurements were sparse in space, showing only a single tracer tongue spreading to the east [*Weiss et al.*, 1985], the recent more detailed measurements, i.e., with higher spatial density, begin to show a similar rich structure of tracer tongues in the middepth equatorial Atlantic as the alternating zonal flow structure of the direct velocity observations suggests. In fact, several off-equatorial tongues, extending up to 10° north and south of the equator, show up as well in the later CFC observations [*Andrie et al.*, 1999].

[4] Similar to the early CFC observations, ocean general circulation models of the Atlantic Ocean at eddy-permitting resolution tend to show a broad tongue high in salinity along the equator in middepths, while such tracer structures are not present at lower resolution [*Böning and Schott*, 1993]. However, this tongue gradually decreases with longer integration time and its presence depends crucially on subgrid-scale parameterization schemes [*Kröger*, 2001]. In this paper, it is shown that, similar to the recent CFC observations, models with increased horizontal resolution (eddy resolving) also reveal a much richer structure of such tongues in various tracers extending into the subtropical Atlantic. Furthermore, an analysis of float trajectories yields

[1]Leibniz-Institut für Meereswissenschaften an der Universität Kiel, Kiel, Germany.

0148-0227/06/2006JC003565$09.00

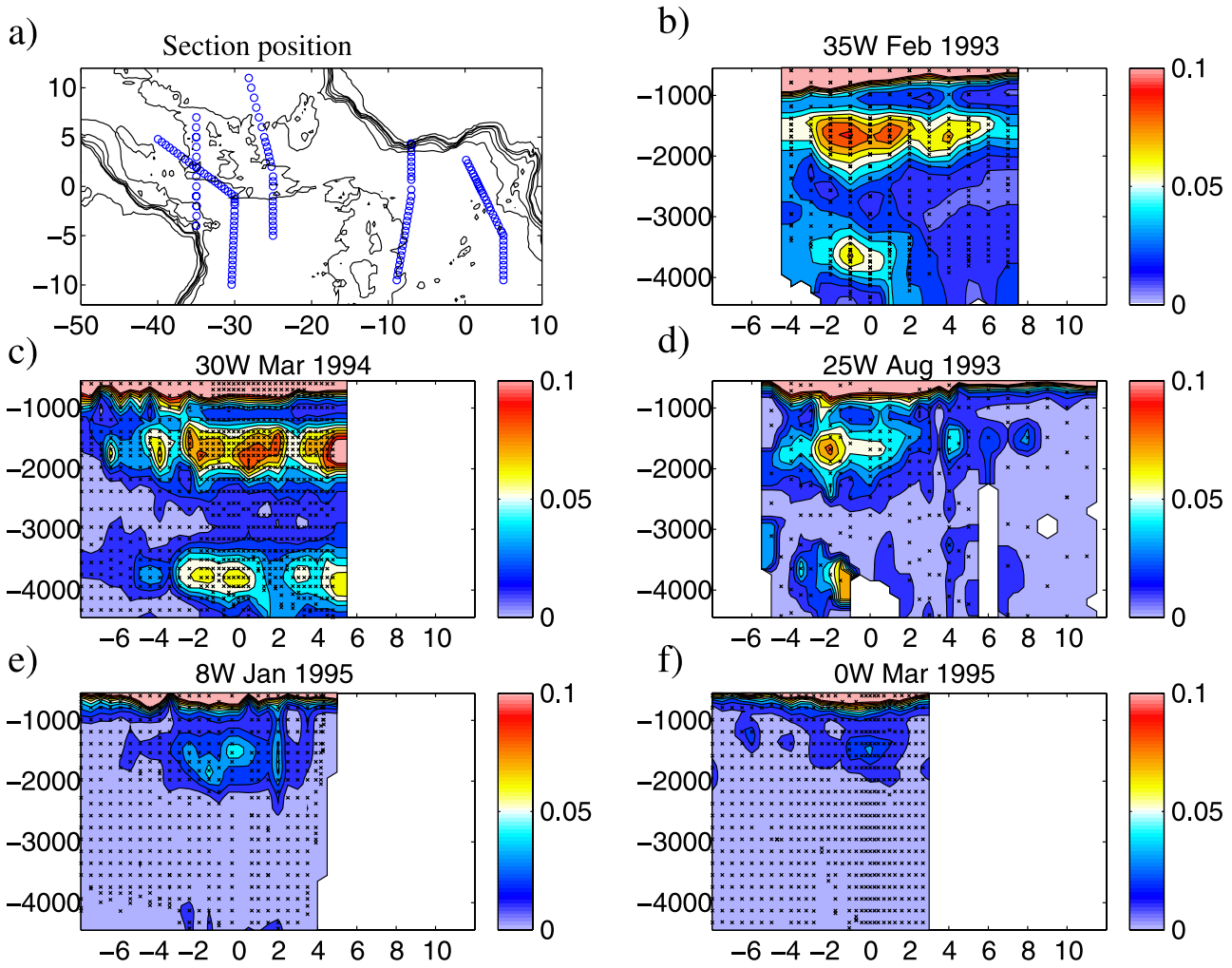

Figure 1. CFC-11 concentration in pmol/kg at different zonal sections and years from GLODAP. Rough longitudinal locations and times are denoted on the figures. (a) Profile positions of the sections. (b, c, d, e, f) Actual data points (crosses).

estimates of the transport fractioning between the eastward flow into the interior basin and the southward, cross hemispheric DWBC.

[5] The tracer tongues are part of a basin-wide system of alternating zonal currents as found now in several eddy-resolving model simulations [*Treguier et al.*, 2003; *Nakano and Hasumi*, 2005; *Maximenko et al.*, 2005; *Richards et al.*, 2006]. The forcing mechanism of these jets, however, is under debate: while *Treguier et al.* [2003] suggest a linear wind driven response being responsible for the zonal jets near the equator, *Galperin et al.* [2004], *Nakano and Hasumi* [2005], and *Maximenko et al.* [2005] suggest an eddy-driven mechanism forming these jets, characteristic of geostrophic turbulence on a β plane [*Rhines*, 1977]. Here, the dependency of the strength of the zonal jets to the choice of subgrid-scale parameterization are explored using sensitivity experiments, pointing toward a strong dependency on the amount of diapycnal mixing in the model.

[6] Beginning with a review of observational evidence for the middepth tracer tongues by presenting several published CFC sections in the equatorial Atlantic Ocean in section 2, it is shown in section 3 that similar tongues show up in the middepth equatorial Atlantic in different tracers in an eddy-resolving model of the Atlantic. In section 4 transport fractioning of the flow of the DWBC into the interior (jets) and into the South Atlantic in the model is estimated. In section 5 model dependencies of the amplitudes of the middepth zonal jets are discussed to infer possible generation mechanism in the model. The last section concludes with a discussion of the results.

2. Observational Estimates of Tracer Tongues

[7] In this section, the observational evidence for the existence of zonal jets in the equatorial Atlantic Ocean is shortly reviewed in order to connect to the model results. Figure 1 displays a compilation of observational estimates of CFC-11 concentrations in zonal sections in the middepth equatorial Atlantic from the early 1990s. The data have been downloaded as quality controlled bottle data from the GLODAP [*Sabine et al.*, 2004] Web site (http://cdiac.esd.ornl.gov/oceans/glodap/Glodap_home.htm). All sections have been regridded on a 100 m $\times$ 0.5° grid by optimal interpolation using a radius of influence of 100 m and 1/5°

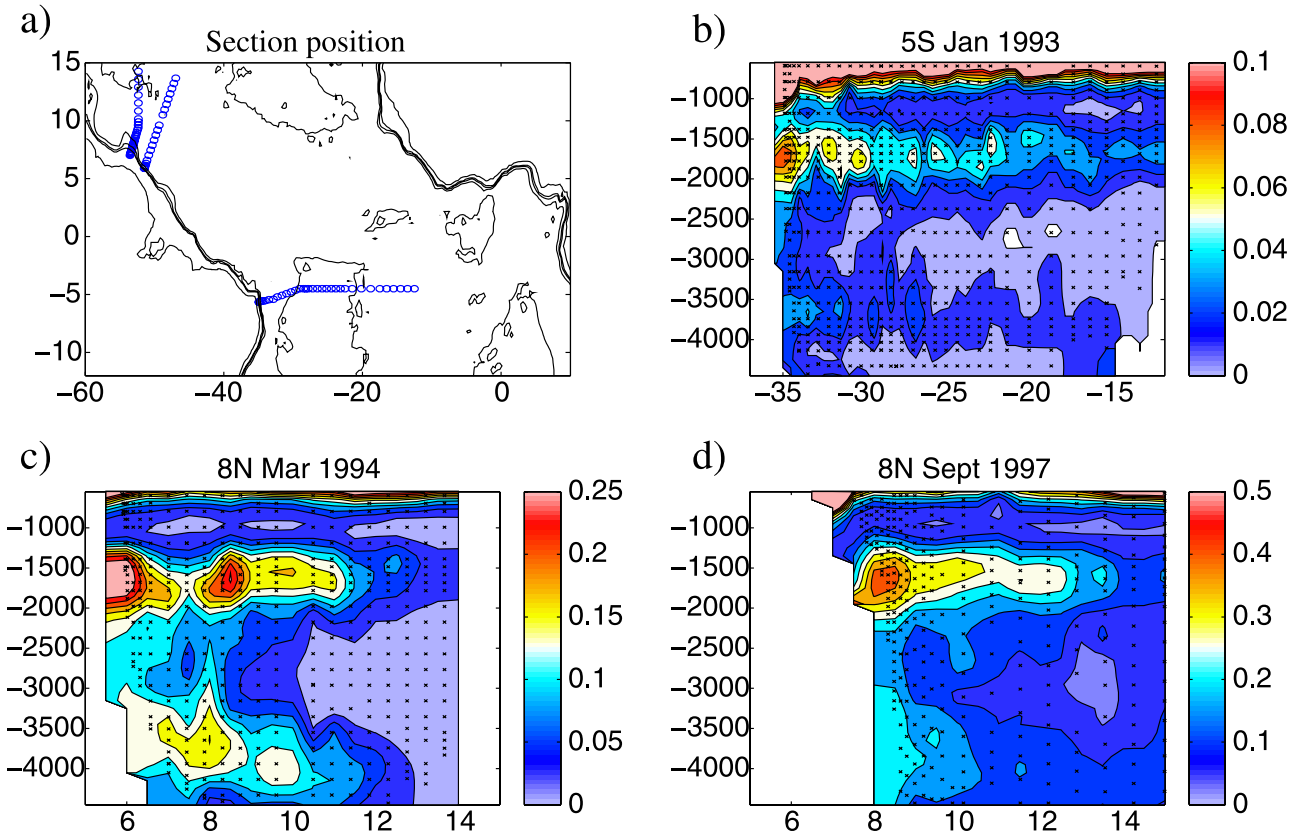

Figure 2. CFC-11 concentration in pmol/kg at different sections from GLODAP. (a) Profile locations of the sections. (b, c, d) Actual data points (crosses).

and four times larger cutoff radius. Note that the individual sections have been discussed, e.g., by *Rhein et al.* [1995], *Outdot et al.* [1998], and *Andrie et al.* [1998, 1999].

[8] Below the CFC rich thermocline, local middepth maxima around 1500–2000 m are evident in all sections. In addition, deep maxima around 3500–4000 m depth show up in the sections west of 25°W (which are not further discussed here). In general, the middepth maxima tend to be larger to the west and toward the equator. In the section along 35°W, these maxima are located at 1°–2° north and south of the equator while a weaker one can be located around 4°–5°N. At 30°W the equatorial maxima at 1–2° north and south of the equator and at 4°–5°N are present as well and, in addition, distinct maxima around 4°S and 6°S show up. At 25°W the maximum at 1°–2° south is larger compared to its northern counterpart, maxima at 4°N and 4°S can be found as well, with, however, much weaker magnitudes compared to the western sections. Further to the north concentrations are much lower, although another, weaker maximum is located at 8°N and a profile at 6°N might be interpreted as another local maximum. The sections to the east show much lower CFC-11 concentrations, but with maxima 1°–2° of the equator.

[9] Overall, the observational estimates suggest a series of CFC-11 rich zonal jets in the middepth equatorial Atlantic, separated by about 2° in latitude, transporting high CFC-11 concentrations from the western boundary current into the interior equatorial Atlantic. There appears to be no jet directly at the equator and the transport of the zonal jets appears to be stronger toward the equator.

[10] Clearly, the CFC-rich water stems from the DWBC, but how large is the concentration in the western boundary current compared to the interior concentration? Figure 2 shows middepth CFC-11 concentrations at a section along 5°S in 1993. Since this section is located just south of the jets along 4°N as seen in the section along 30°W in Figure 1c in 1994, the zonal extent of the jet can be traced into the interior of the Atlantic. Consistent with the zonal section, concentrations are decreasing to the east. At the western boundary CFC-11 concentrations are highest with, however, similar magnitudes as seen in the zonal sections at the equator. Upstream, CFC-11 concentrations are much higher. Figures 2c and 2d show sections across the deep western boundary current roughly at 8°N. Note the different color range. In 1994, middepth CFC-11 concentrations are more than two times larger than in the jets at the equator and south of the equator a year before. Note also the local maximum in CFC-11 at 8°N in Figure 2c, which can also be seen as a (weak) local maximum in Figure 1d at 25°W at the same latitude a year before. Note that there is a strong time tendency at this location since three years later concentrations are two times higher than 1994 at 8°N.

[11] However, as long as we assume that the meridional section in Figure 2b samples correctly the CFC-11 rich signal in the western boundary current, we might conclude that in 1993/94 concentrations in the western boundary south of the equator are of similar magnitude than in the

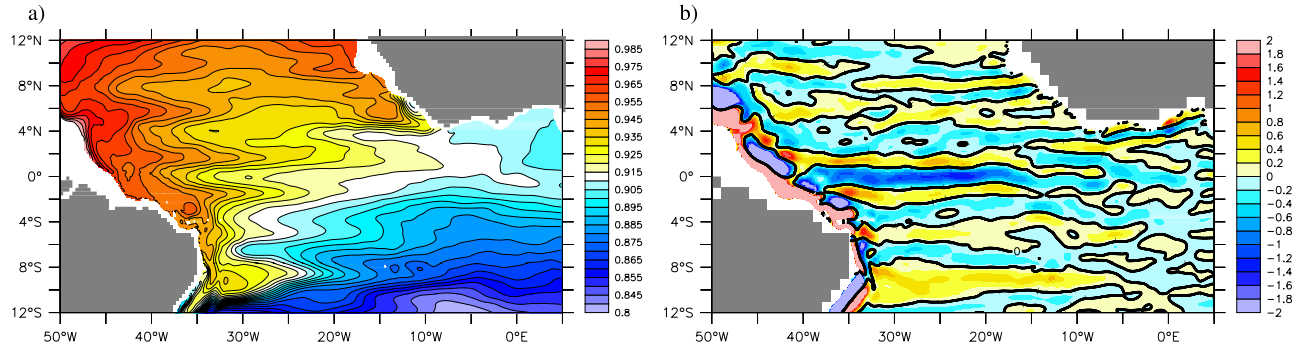

Figure 3. (a) The 3-year mean salinity minus 34.0 psu and (b) 3-year mean zonal velocity (in cm/s) in 1500 m depth in an eddy-resolving (1/12°) model of the Atlantic Ocean.

zonal jets in the interior of the equatorial Atlantic (Figure 1b). This suggests that equatorial transports in this depth range toward the interior and to the south along the western boundary are of similar magnitudes.

3. Tracer Tongues in a Model

[12] Results from an eddy-resolving model of the Atlantic Ocean are shown and compared to the CFC observations in this section. The horizontal resolution (1/12°) of this model is about 10 km at the equator decreasing to about 5 km in high latitudes. The model domain extents from 20°S to 70°N with open boundaries [*Stevens*, 1990] at the northern and southern boundaries. (The prescribed stream function data for the northern boundary were made available by the Arctic Modelling Group at AWI Bremerhaven, Germany (R. Gerdes, personal communication, 2004); the stream function for 20°S is the same as in DYNAMO.) and with a buoyancy restoring zone in the eastern Mediterranean Sea. There are 45 vertical geopotential levels with increasing thickness with depth, ranging from 10 m at the surface to 250 m near the maximal depth of 5500 m. Surface boundary forcing is given by monthly mean wind stress, a Haney-type heat flux condition as given by *Barnier et al.* [1995] and a restoring condition for sea surface salinity. Subgrid-scale parameterization are biharmonic friction and diffusion (with diffusivity of 0.8×10^{10} m^4/s and viscosity of 2×10^{10} m^4/s) and a closure for the vertical turbulent kinetic energy (TKE) following *Gaspar et al.* [1990], utilizing identical parameters as *Oschlies and Garcon* [1999]. The model is based on a rewritten version (FLAME) of MOM2 [*Pacanowski*, 1995] and is identical to the one used by *Dengler et al.* [2004] and *Eden et al.* [2006]. The numerical code together with all configurations used in this study can be accessed at http://www.ifm.uni-kiel.de/fb/fb1/tm/data/pers/ceden/spflame/index.html. The model is integrated for a 10 year spinup period, the results shown here are taken from a subsequent integration of 10 years.

[13] Similar middepth equatorial tracer tongues as in the observations can be found in the model. Since there is no CFC-11 simulation for the model, Figure 3a shows the long-term mean salinity in 1500 m depth in the equatorial Atlantic. Salinity is high in the deep western boundary current related to the local salinity maximum in the depth range of the upper NADW (about 34.95 psu) with a negative horizontal gradient toward the southeast. Superimposed on this large-scale structure are zonal tongues of high salinity reaching from the salty deep western boundary current into the fresher interior Atlantic.

[14] Figure 3b shows the mean zonal velocity for the same depth level in the model. Eastward zonal jets centered about 1°–2° latitude north and south of the equator of about 1 cm/s fall together with the high-salinity tongues off the equator in Figure 3a at the same latitude. Between both eastward jets, westward zonal flow of about −1.5 cm/s can be found, related to the relative salinity minimum at the equator. Further eastward jets and high-salinity tongues are roughly located at the latitudes 6°N, 10°N, 4°S and 8°S. The mean zonal velocity related to the mean zonal jet structures is rather low compared to, e.g., the deep western boundary current, however apparently strong enough to sustain the salinity tongues. Note that structures as the salinity tongue cannot be found in the initial conditions of the model [*Boyer and Levitus*, 1997] since observational noise is dominating the horizontal pattern (not shown). This means that the zonal jets are brought about by the internal oceanic dynamics and become a robust feature of the evolving flow field during the spin up.

[15] Similar tracer tongues as in salinity also show up in various other tracers in the model. Figure 4 shows dissolved oxygen and inorganic carbon (DIC) in 1500 m depth of the same eddy-resolving model as in Figure 3. These tracers are calculated coupling a simple pelagic ecosystem and carbon cycle model to the general circulation model. The ecosystem/carbon chemistry model is the same as in work by *Eden and Oschlies* [2006] and was integrated coupled to the eddy-resolving model for 15 years. Figure 3 shows the annual mean of the last year. There are in both tracers large-scale gradients between the DWBC and the interior; the DWBC is richer in oxygen and lower in DIC than the interior tropical Atlantic in this depth range because of the interaction of different ventilation timescales and biological carbon drawdown and oxygen utilization. Near the equator and the DWBC, tracer tongues at the same locations and with a similar zonal extent as before for salinity show up. Note that as before for salinity, these structures are not present in the initial conditions for oxygen or DIC (not shown), pointing toward a significant transport associated with the zonal jets.

[16] Figure 5 shows two meridional sections of different tracers and zonal velocity in the depth range of the equatorial tracer tongues. Figures 5a and 5b shows salinity at

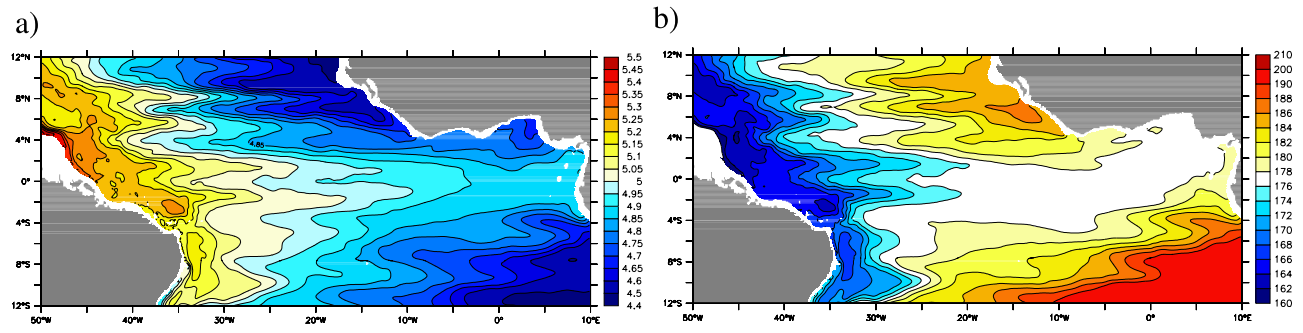

Figure 4. (a) The 3-year mean dissolved oxygen (ml/l) in 1500 m depth and (b) 3-year mean dissolved inorganic carbon (mmol/m^3 − 2000) concentrations in the eddy-resolving (1/12°) model.

30°W and 20°W, respectively. There is saltier water compared to the surrounding associated with the cores of zonal jets in 1500 to 2000 m. Although weaker in amplitude at the eastern section, the same structure in salinity shows up at both sections. Furthermore, the local maxima fall together with eastward zonal velocity in this depth range. Figure 5c shows oxygen at 30°W and Figure 5d shows DIC at 20°W. The water rich in oxygen and low in DIC from the DWBC shows up at both sections, very similar to the CFC sections shown in Figures 1 and 2. Note that below about 2000 m similar tracer signals related to zonal jets cannot be found. On the other hand, the Figures 5a and 5b show zonal flow with a jet-like structure also below 2000 m. The missing tracer signal in these flow structures is related to the fact that

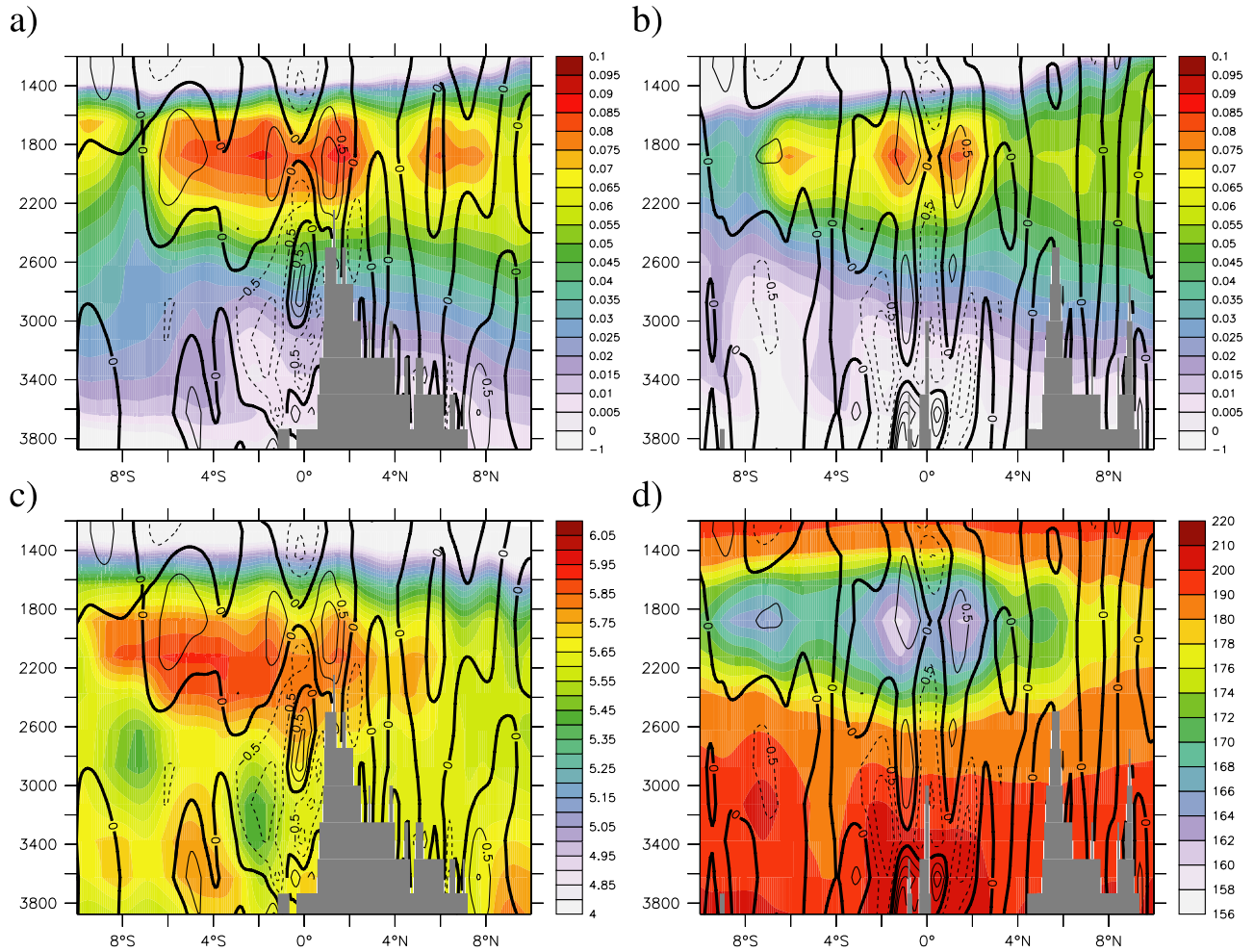

Figure 5. The 3-year mean salinity minus 34.9 psu along (a) 30°W and (b) 20°W, (c) mean dissolved oxygen in ml/l at 30°W, and (d) mean dissolved inorganic carbon in mmol/m^3 − 2000 in the 1/12° model. Also shown are isotaches of the mean zonal velocity from −2 cm/s to 2 cm/s using 0.5 cm/s contour spacing.

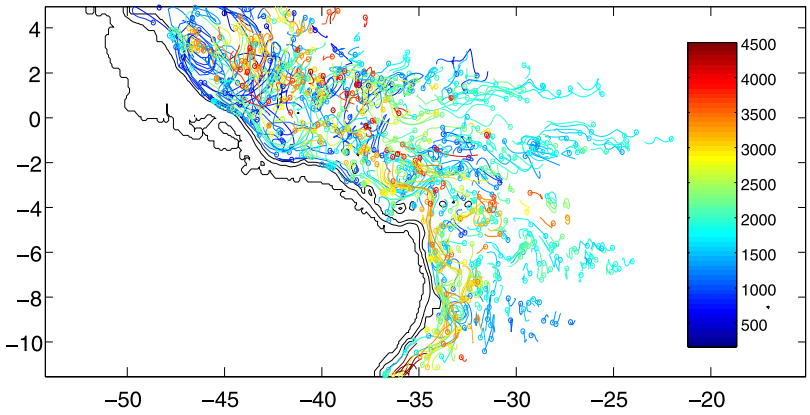

Figure 6. Neutrally buoyant particles integrated for 5 years in the 1/12° model. Particles are deployed at 4°N in the deep western boundary current. Shown are end positions (dots) and trajectories of the last 45 days (lines). Color coding denotes depth.

there is also no such tracer signal near the western boundary below 2000 m, in contrast to the depth range of 1500–2000 m, where the DWBC carries such anomalous tracer signals.

4. Advective Transports in the Tracer Tongues

[17] Clearly, the tracer tongues are an imprint of a zonal transport from the western boundary toward the interior of the equatorial Atlantic. In the model, such a transport can be generated by either lateral diffusion of the subgrid-scale parameterizations or by advection. Note that the latter process is of turbulent nature, which is sometimes parameterized or viewed as turbulent diffusion, [see, e.g., *Bartello and Holloway*, 1991]. Here, however, the aim is to quantify the advective transport associated with the zonal jets, either by mean advection or by the resolved turbulent flow field, excluding any effects of the (diffusive) subgrid-scale parameterization (which might be wrong).

[18] To quantify the Lagrangian transport and to differentiate between effects of diffusion and advection, trajectories of neutrally buoyant particles integrated for 5 years in the instantaneous velocity field of the model are discussed in this section. Figure 6 shows the end points of the particles, which are released at 4°N at the shelf distributed from 1000 m to 3500 m on 1 January. It is evident from Figure 6 that indeed many particles make their way into the zonal jets at 1°–2° north and south of the equator in the depth range 1500–2000 m. The particles which end up in the jet at 4°S tend to be deeper, the ones in the jet at 6°S again predominantly in 1500–2000 m and the particles in the jet at 8°S tend to be shallower. South of 8°S no zonal excursion of particles can be found. Here, the deep western boundary current breaks up into coherent eddies [*Dengler et al.*, 2004].

[19] To quantify the transport related to the amount of particles ending up in the interior zonal jets, it is possible to relate the particles with volume transport following the approach by [*Döös*, 1995]. Each particle is assigned a fraction of the meridional transport of the model grid box in which it has been released. The fraction of the transport is simply given by the number of particles in the particular grid box at the start of the integration of their trajectories. Figure 7 shows the instantaneous meridional velocity at the start points of the particles at 4°N. Although it was tried to place the particles in the deep western boundary current, this definition is somewhat arbitrary since there are strong recirculations (in the instantaneous as well as the mean fields) evident in the velocity section. Also shown in Figure 7

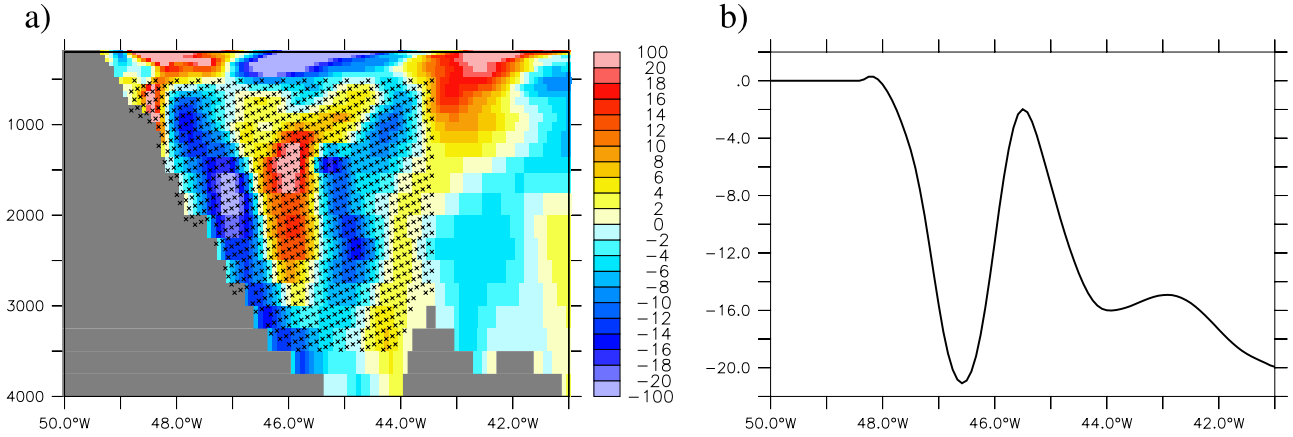

Figure 7. (a) Instantaneous meridional velocity in cm/s at 4°N and start points of particles. (b) Instantaneous cumulative transport in Sv at 4°N between 1000 and 2500 m depth.

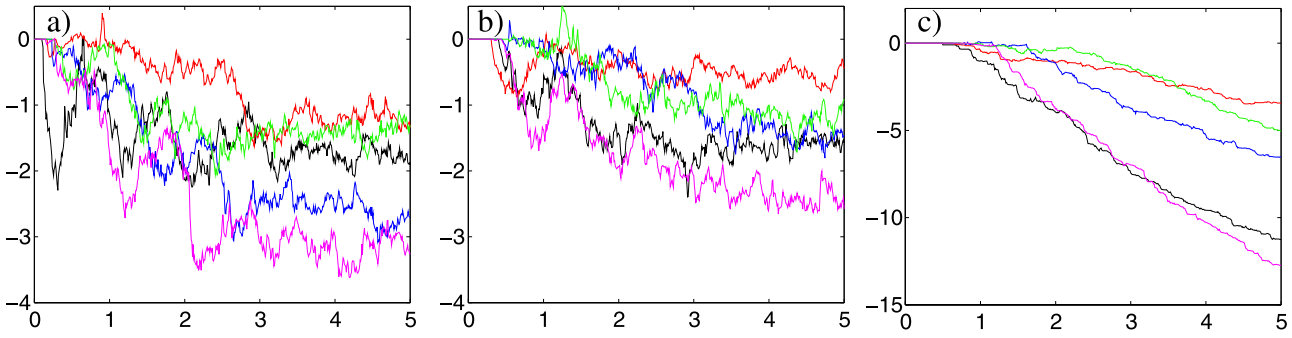

Figure 8. (a) Particle transports in Sv in the region -2500 m $> z > -1000$ m, $0° > y > 3.5°$N, and $-40°$W $< x$ as a function of time from release in years. Different colors denote different release times, i.e., 1 January (black), 1 April (red), 1 July (blue), 1 October (green), and 1 January of the following year (magenta). (b) Particle transports in the region -2500 m $> z > -1000$ m, $4°$S $> y > 0°$N, and $-35°$W $< x$. (c) Particle transports in the region south of 12°S.

is the cumulative transport in the depth range of the deep western boundary current from 1000 m to 2500 m indicating nearly a compensation of the southward transport at the shelf of about 20 Sv by northward flow between 47°W and 45°W. The particles are placed over the southward flow at the shelf as well as the recirculation region and, for the purpose of this analysis, all northward-southward transports occurring between the shelf and 43.5°W are defined as the transport of the deep western boundary current at this section. This longitude was chosen since east of 43.5°W the cumulative transport of the deep western boundary current shows no large fluctuations (compared to west of 43.5°W).

[20] A first group of particles (10000) was released on 1 January of an arbitrary model year after the spinup of the model. The sum of the (southward) transport of all these particles is 27.1 Sv. After 5 years, 11.3 Sv have passed 12°S, whereas the rest (15.8 Sv) stays in the domain between 12°S and 4°N. Of the remaining southward transport north of 12°S, 1.9 Sv resides in jets just north of the equator defined by the region $0° > y > 3.5°$N and $-40°$W $< x$ between 1000 m and 2500 m depth. In addition, 1.6 Sv of the transport resides in the jet just south of the equator, i.e., between $4°$S $> y > 0°$N and $-35°$W $< x$ and -2500 m $> z > -1000$ m.

[21] However, these numbers change repeating the particle releases at later times, because of eddy activity involving these particles. Figure 8 shows time series of the deep western boundary current transport ending up in the jets off the equator and south of 12°S calculated from five groups of particles (10000 each) released in three months distance in time. The transport in the northern equatorial jet ranges between 1.3 Sv and 3.3 Sv after 5 year integration, while its southern counterpart ranges between 0.5 Sv and 2.6 Sv. The time series show that these transport values are already established after 2 to 3 years. In contrast, the transport south of 12°S increases steadily with time, with transport values after 5 years of 3.4 to 12.7 Sv while after 2 to 3 year integration there is an almost equal amount of transport in the off-equatorial jets and south of 12°S. However, there is no clear correlation between the amount of transport south of 12°S and transport ending up in the equatorial jets in the interior. The transport in the jets at 4°S and 8°S are in general lower than the off-equatorial ones.

[22] The zonal Lagrangian mean velocities (not shown) calculated from all floats show only slightly larger (2–3 cm/s) magnitudes than the Eulerian mean velocities in the core of the jets north and south of the equator. Therefore the Eulerian mean velocities can be used as a good indicator for the position and strength of the eastward zonal jets. However, while the zonal Eulerian mean velocities directly at the equator (Figure 3b) show westward flow of about 2 cm/s, the Lagrangian mean velocities show no flow or even small eastward flow. There is apparently no westward transport related to the Eulerian mean westward jets between the eastward ones. This finding is supported by the CFC measurements, which also show CFC directly at the equator in any section which must originate from the DWBC.

5. Model Dependencies

[23] The mechanism generating the equatorial zonal jets might be assessed by considering sensitivity experiments with the model. Figure 9 shows mean salinity in 1700 m depth (after the 10 year spinup) in three different versions of the model. Figure 9a) shows results from a model in which the biharmonic diffusion was replaced by the *Redi* [1982] diffusion tensor together with harmonic background diffusivity of $A_h = 1$ m^2/s while Figure 9c) shows results from a model version with increased biharmonic diffusion, i.e., $A_h = 2.7 \times 10^{10}$ m^4/s instead of $A_h = 0.8 \times 10^{10}$ m^4/s as for the standard case shown in Figure 9b).

[24] All other model parameters are left unchanged with the following exceptions: For case a, a Bottom Boundary Layer parameterization is included and the vertical diffusivity parameterization is changed to the one proposed by *Gargett* [1984] which, however, leads to only slightly higher vertical diffusivities in the region of interest. For case b, enhanced viscosity, i.e., $A_h = 2.7 \times 10^{10}$ m^4/s instead of $A_h = 2 \times 10^{10}$ m^4/s as for cases a and b is used, with however minor influence on mesoscale activity. Overall, the main difference in the three model experiments is given by changes in the lateral diffusion scheme acting on temperature and salinity. As pointed out first by *Veronis* [1975] lateral diffusion along geopotentials, as in cases b and c,

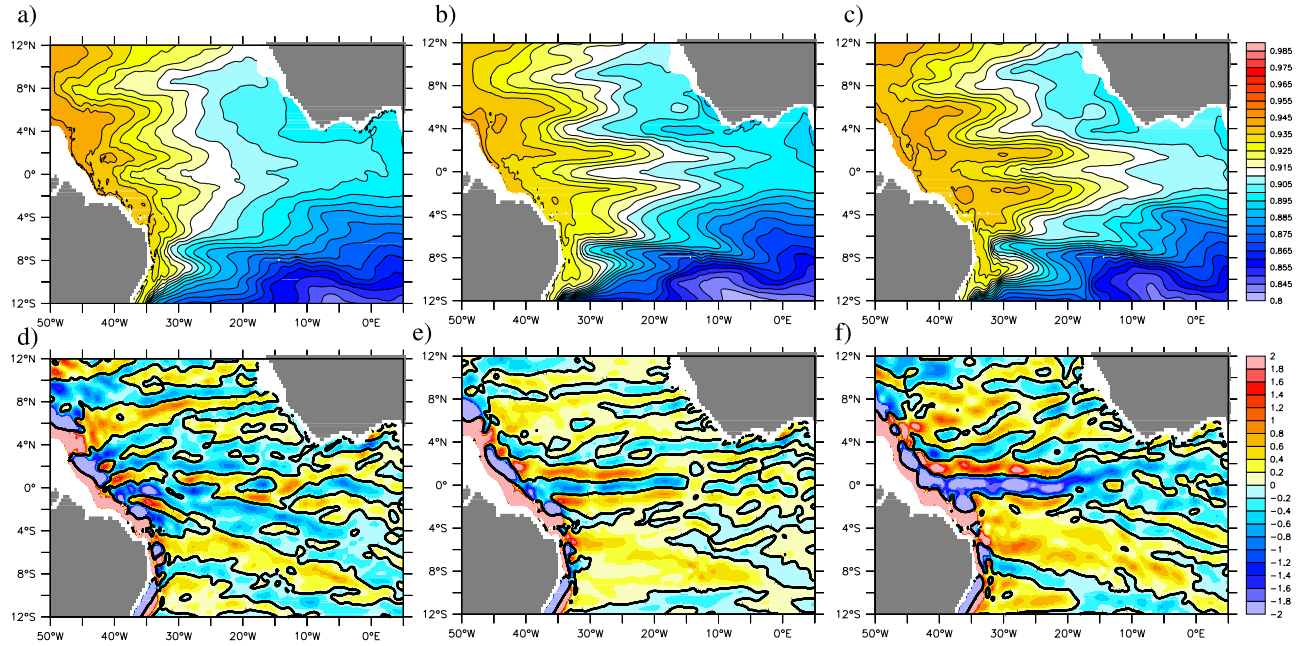

Figure 9. (a, b, c) The 3-year mean salinity minus 34.05 psu and (d, e, f) 3-year mean zonal velocity (cm/s) in 1700 m depth in a 1/12° model version with reduced diapycnal diffusivity (Figures 9a and 9d), with normal diffusivity (Figures 9b and 9e), and with enhanced diffusivity (Figures 9c and 9f).

leads to a diapycnal projection of the diffusion fluxes. This artifact is much reduced using lateral diffusion along isopycnals, as in case a. Note that there are also other effects due to the numerical representation of advection which might increase the effective diapycnal diffusivities in eddy-resolving models, [see, e.g., *Griffies et al.*, 2000; *Lee et al.*, 2002], but it is beyond the scope of the present paper to exactly quantify the amount of effective diapycnal mixing. However, because of the Veronis effect, case c should be most and case a least diapycnally diffusive.

[25] The results from the different model experiments are somehow counter intuitive. For the most diffusive model (case c), the strongest imprint in salinity by the zonal jets can be seen. Note that the salinity in the deep western boundary current and in the eastern equatorial Atlantic is the same in all model versions. Therefore it appears not to be a possible change in the large-scale salinity distribution which is responsible for the model difference. The relation between the subgrid-scale mixing in the model and the strength of the jets is also supported by a look at the mean zonal velocities in the different models, shown in Figures 9d, 9e, and 9f. The position and strength of the zonal jets coincide again with the salinity tongues (similar to Figure 3) in each of the experiments. The stronger the zonal velocities, the stronger the salinity signal in the equatorial tongues.

[26] In the above section, it was found that there is considerable Lagrangian tracer transport related to the zonal jets. Furthermore, the colocation of both tracer tongues and mean zonal advection, i.e., jets, in each of the sensitivity experiments also suggest that advection (and not subgrid-scale diffusion) is creating the salinity tongues in the models. On the other hand, the salinity flux related to isopycnal diffusion in case a is certainly (on mean isopycnals, which are almost flat in this region) much stronger than its biharmonic counterpart in case b and c. However, this diffusive flux is obviously not efficient enough to move much salty water from the deep western boundary current into the fresh interior, since otherwise the large-scale salinity gradient in case a would differ from the other cases.

[27] The amplitude of the tracer tongues are thus dominantly given by advective effects, i.e., the strength of the jets. The impact of the different subgrid-scale parameterization on the strength of the jets are given by their effect on density, i.e., by the amount of diapycnal diffusion in the different model versions (besides complications with the nonlinear equation of state, which are neglected here). It is therefore concluded on the basis of the model experiments that more diapycnal mixing is related to stronger jets.

6. Discussion

[28] Observational evidence for middepth tracer tongues in the equatorial Atlantic, as first proposed by *Weiss et al.* [1985], has been reviewed and compared with results from three different eddy-resolving model simulations, which show good agreement to the observations. Strongest imprint of the eastward jets in simulated tracers such as salinity, oxygen and DIC and observed CFC are found 1°–2° off the equator, further eastward jets are located around 4°–6°N/S and 8°–10°N/S, although with a weaker signal in the CFC measurements and the simulated tracer distributions. Lagrangian transport estimates in the model using float diagnostics show a fluctuating transport of 1–3 Sv in each of the eastward jets 1°–2°N/S off the equator compared to 3–12 Sv throughflow into the South Atlantic. There was no seasonal cycle apparent in the transport fractioning and the transport in the jets at 4°–6°N/S and 8°–10°N/S is lower compared to the eastward jets 1°–2°N/S off the equator. In the model, these jets are part of a basin-wide system of alternating jets, as

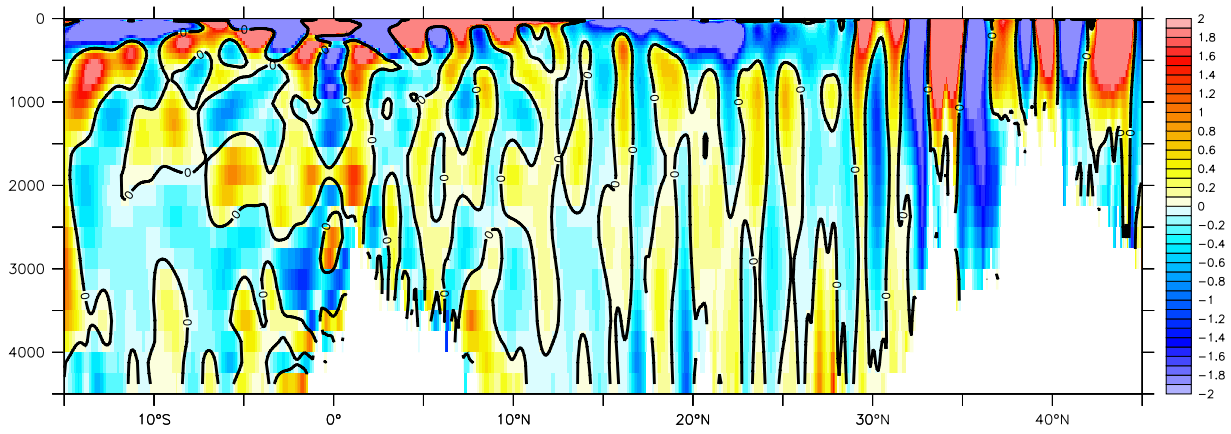

Figure 10. The 3-year mean zonal velocity along 30°W in cm/s in the North Atlantic.

evident in Figure 10 showing the mean zonal velocity at 30°W. Jets with velocities of 1–2 cm/s show up in the entire North Atlantic, with a separation scale similar to the equatorial ones.

[29] Such jets are not a special feature of this particular model or the Atlantic Ocean: *Nakano and Hasumi* [2005] and more recently *Richards et al.* [2006] find similar jet structure in models of the Pacific Ocean with a similar meridional structure, i.e., 1°–2° separation scale. *Treguier et al.* [2003] show evidence for similar jets in the South Atlantic from floats and an eddy-permitting model. *Maximenko et al.* [2005] analyzed satellite sea surface elevation data and a global eddy-resolving model and find also similar zonal jets in all oceans both in the model and the data. Recently, similar middepth zonal jets near the equator has also been found in a compilation of float data in the Atlantic Ocean by *Ollitrault et al.* [2006].

[30] It should be mentioned that such zonal jets cannot be found in coarser resolution models (i.e., with grid spacings larger than the local Rossby radius), and that the initial conditions for the present model do not contain any information about the equatorial tongues in salinity, oxygen or DIC. This means that the zonal jets are brought about by the internal mesoscale oceanic dynamics and become a robust feature of the evolving flow field during the spin up. Even though the velocities associated with the jets are only of the order of 1 cm/s, they still leave a profound signature on the distribution of several independent tracers.

[31] What is the driving mechanism of the jets? *Treguier et al.* [2003] suggest a frictionally arrested wind driven response being responsible for a large part of the flow structure in the tropical ocean, including the zonal jets. They argue, on the basis of idealized model experiments, that the response of the linear wave dynamics on the wind stress forcing the tropical ocean, is able to provide the complicated zonal flow structure, including the zonal jets, when it is arrested by vertical friction or diffusion. This suggestion was also further investigated by *Nakano and Hasumi* [2005] for a model simulation of the tropical Pacific Ocean.

[32] However, following *Rhines* [1975, 1977], *Galperin et al.* [2004], *Nakano and Hasumi* [2005] and more recently *Maximenko et al.* [2005] suggest an alternative eddy-driven mechanism of the jets' formation. *Galperin et al.* [2004] compare the model results of *Nakano and Hasumi* [2005] with the famous pronounced band structure in Jupiter's disk and other planets of the solar system. They argue that similar spectral characteristics of the flow on the planets and in the ocean points toward a similar dynamical mechanism, i.e., geostrophic turbulence on a β plane [*Rhines*, 1975, 1977]. Here, small-scale forcing is necessary to invoke an inverse energy cascade to larger, anisotropic scales, forming the banded flow structures on Jupiter and also the oceanic zonal jets on earth as suggested by *Galperin et al.* [2004]. In the ocean, the small-scale forcing is thought to come from energy released (adiabatically) by baroclinic and barotropic instability from the mean available potential energy [*Larichev and Held*, 1995]. On Jupiter, there is also the possibility of diabatic forcing on the small scales coming from thermal convection by heating from below [*Galperin et al.*, 2004]. However, the energy cycle in the ocean remains currently largely unknown [*Wunsch and Ferrari*, 2004], and it is beyond the scope of this paper to speculate about it, but recent experimental work [*Read et al.*, 2004] points toward the importance of small-scale forcing in energy and enstrophy cascades also for the ocean.

[33] It should also be mentioned that the basinwide system of jets (Figure 10) shows a tendency to become equivalent barotropic off the equator; that is, the subsurface flow direction inside the jets remains the same throughout the water column. A similar feature was found in a model of the Pacific Ocean by *Richards et al.* [2006] and is an important feature of geostrophic turbulence on a β plane as discussed by *Galperin et al.* [2006]. This finding points to a possible dynamical difference between the equatorial and off-equatorial jets, as the former show a strongly baroclinic structure. *Nakano and Hasumi* [2005] suggest a superposition of a wind driven frictionally arrested wave response with a strong baroclinic structure as suggested by *Treguier et al.* [2003] with jets formed by geostrophic turbulence to explain the complicated zonal flow structure in the tropical Pacific Ocean.

[34] The model dependencies discussed here show that stronger diapycnal mixing is related to stronger jets. Since it is known from the CFC observations that there are zonal jets, connecting the DWBC with the interior Atlantic, and that there is significant transport related to these jets, the surprising result is that the more diffusive model is in better agreement with the observations, since the more diffusive

models show stronger imprints in the middepth salinity tongues. It might be speculated that the (diabatic) release of mean potential energy by diapycnal mixing is responsible to enhance the equatorial zonal jets in the model. However, note that this (artificial) diapycnal mixing [*Veronis*, 1975] feeds from potential energy which is normally unavailable to adiabatic processes. Note also, that strengthened zonal jets in response to increased diffusion or damping is also observed for general circulation models of the atmosphere [*Held and Phillips*, 1993]. *Robinson* [1997] explains this nonlinear behavior by the fact that stronger diffusion is able to enhance and to localize eddy momentum fluxes, which in turn accelerate the mean zonal flow.

[35] The above described model dependency might be taken as a hint toward enhanced diapycnal diffusivity related to these jets. On the other hand, this finding is in strong disagreement of direct turbulence measurements, which show generally much lower diffusivities below the thermocline and in particular a pronounced minimum in equatorial regions [*Gregg et al.*, 2003], suggesting very low diapycnal mixing here. However, it is possible to speculate that these measurements only show small time slices of the turbulence field, while intermittent events, resulting from, e.g., static instabilities induced by the flow itself, could well be missed. In fact, *d'Orgeville et al.* [2004] found layers of constant densities of 50–100 m thickness in hydrographical sections within 2° off the equator below the thermocline. They argue that static instabilities can be generated by inertial instability of the zonal (oscillating) background flow and that strong vertical mixing due to these static instabilities might be a plausible mechanism for this strong layering. On the other hand, it was argued that such layers can also be generated by adiabatic layer thickness convergence and divergence due to linear wave activity [*Dengler and Quadfasel*, 2002].

[36] To conclude, the question of the driving mechanism of the zonal jets and the amount of diapycnal mixing in the interior equatorial ocean remains open here, but it is shown that the horizontal flow in eddy-resolving numerical models is very sensitive to diapycnal mixing, which is in most cases artificial and influenced by subgrid-scale parameterizations and numerical schemes and can obscure the interpretation of model results. It should be noted that the models used in the studies by *Nakano and Hasumi* [2005], *Maximenko et al.* [2005], and *Treguier et al.* [2003] are very similar to the present one and suffer from the same numerical problems, maybe even more in case of coarser resolution. Therefore it is stressed here that the interpretation of model results and inference of possible forcing mechanism of (weak) zonal jets in the interior of the ocean require caution. However, as demonstrated from observations and model results, there is significant transport along the equator into the interior of the ocean associated with the equatorial jets. This transport should be included in climate models to improve simulations of southward spreading transient tracer signals.

[37] **Acknowledgments.** This work was supported by the European Union within the project DYNAMITE. Two anonymous reviewers helped to improve the manuscript. The model integrations have been performed on a SGI-ALTIX and a NEC-SX8 at the computing center at the University of Kiel, Germany, and on a NEC-SX6 at the Deutsches Klimarechenzentrum, Hamburg, Germany.

References

Andrie, C., J.-F. Ternon, M.-J. Messias, L. Memery, and B. Bourles (1998), Chlorofluoromethane distribution in the deep equatorial Atlantic during January–March 1993, *Deep Sea Res., Part I*, *45*, 903–930.

Andrie, C., J.-F. Ternon, B. Bourles, Y. Gouriou, and C. Oudot (1999), Tracer distributions and deep circulation in the western tropical Atlantic during CITHER 1 and ETAMBOT cruises, 1993–1996, *J. Geophys. Res.*, *104*, 21,195–21,215.

Barnier, B., L. Siefridt, and P. Marchesiello (1995), Thermal forcing for a global ocean circulation model using a three year climatology of ECMWF analysis, *J. Mar. Syst.*, *6*, 363–380.

Bartello, P., and G. Holloway (1991), Passive scalar transport in beta-plane turbulence, *J. Fluid Mech.*, *223*, 521–536.

Böning, C., and F. Schott (1993), Deep currents and the eastward salinity tongue in the equatorial Atlantic: Results from an eddy-resolving, primitive equation model, *J. Geophys. Res.*, *98*, 6991–6999.

Boyer, T. P., and S. Levitus (1997), Objective analyses of temperature and salinity for the world ocean on a 1/4 degree grid, technical report, *NOAA Atlas NESDIS 11*, NOAA, Silver Spring, Md.

Brandt, P., and C. Eden (2004), Annual cycle and interanual variability of the mid-depth tropical Atlantic Ocean, *Deep Sea Res., Part I*, *52*, 199–219.

Dengler, M., and D. Quadfasel (2002), Equatorial deep jets and abyssal mixing in the Indian Ocean, *J. Phys. Oceanogr.*, *32*, 1165–1180.

Dengler, M., F. A. Schott, C. Eden, P. Brandt, J. Fischer, and R. J. Zantopp (2004), Break-up of the Atlantic deep western boundary current into eddies at 8°S, *Nature*, *432*, 1018–1020.

Döös, K. (1995), Interocean exchange of water masses, *J. Geophys. Res.*, *100*, 13,499–13,514.

d'Orgeville, M., B. L. Hua, R. Schopp, and L. Bunge (2004), Extended deep equatorial layering as a possible imprint of inertial instability, *Geophys. Res. Lett.*, *31*, L22303, doi:10.1029/2004GL020845.

Eden, C., and A. Oschlies (2006), Adiabatic reduction of circulation-related CO_2 air-sea flux biases in a North Atlantic carbon-cycle model, *Global Biogeochem. Cycles*, *20*, GB2008, doi:10.1029/2005GB002521.

Eden, C., R. J. Greatbatch, and J. Willebrand (2006), A diagnosis of thickness fluxes in an eddy-resolving model, *J. Phys. Oceanogr.*, in press.

Galperin, B., H. Nakano, H.-P. Huang, and S. Sukoriansky (2004), The ubiquitous zonal jets in the atmospheres of giant planets and Earth's oceans, *Geophys. Res. Lett.*, *31*, L13303, doi:10.1029/2004GL019691.

Galperin, B., S. Sukoriansky, N. Dikovskaya, P. Read, Y. Yamazaki, and R. Wordsworth (2006), Anisotropic turbulence and zonal jets in rotating flows with a β-effect, *Nonlinear Processes Geophys.*, *13*, 83–89.

Gargett, A. E. (1984), Vertical eddy diffusivity in the ocean interior, *J. Mar. Res.*, *42*, 359–393.

Gaspar, P., Y. Gregoris, and J.-M. Lefevre (1990), A simple eddy kinetic energy model for simulations of the oceanic vertical mixing: Tests at station PAPA and Long-Term Upper Ocean Study site, *J. Geophys. Res.*, *95*, 16,179–16,193.

Gregg, M. C., T. B. Sanford, and D. P. Winkel (2003), Reduced mixing from the breaking of internal waves in equatorial waters, *Nature*, *422*, 513–515.

Griffies, S. M., R. C. Pacanowski, and B. R. Hallberg (2000), Spurious diapycnal mixing associated with advection in a z-coordinate ocean model, *Mon. Weather Rev.*, *128*, 538–564.

Held, I. M., and P. J. Phillips (1993), Sensitivity of the eddy momentum flux to meridional resolution in atmospheric GCMs, *J. Clim.*, *6*, 499–507.

Jochum, M., and P. Malanotte-Rizzoli (2003), The flow of AAIW along the equator, in *Interhemispheric Water Exchange in the Atlantic Ocean*, *Elsevier Oceanogr. Ser.*, vol. 68, edited by P. Malanotte-Rizzoli and G. J. Goni, pp. 193–212, Elsevier, New York.

Johnson, H. L., and D. P. Marshall (2002), A theory of the surface Atlantic response to thermohaline variability, *J. Phys. Oceanogr.*, *32*, 1121–1132.

Kröger, J. (2001), Mechanismen meridionaler Transportprozesse im tropischen Atlantik, Ph.D. thesis, Inst. für Meereskunde, Univ. Kiel, Kiel, Germany.

Larichev, V., and I. Held (1995), Eddy amplitudes and fluxes in a homogenous model of fully developed baroclinic instability, *J. Phys. Oceanogr.*, *25*, 2285–2297.

Lee, M.-M., A. C. Coward, and A. J. Nurser (2002), Spurious diapycnal mixing of the deep waters in an eddy-permitting global ocean model, *J. Phys. Oceanogr.*, *32*, 1522–1535.

Lux, M., H. Mercier, and M. Arhan (2001), Interhemispheric exchanges of mass and heat in the Atlantic Ocean in January–March 1993, *Deep Sea Res., Part I*, *48*, 605–638.

Maximenko, N. A., B. Bang, and H. Sasaki (2005), Observational evidence of alternating zonal jets in the world ocean, *Geophys. Res. Lett.*, *32*, L12607, doi:10.1029/2005GL022728.

Nakano, H., and H. Hasumi (2005), A series of zonal jets embedded in the broad zonal flows in the Pacific obtained in eddy-permitting ocean general circulation models, *J. Phys. Oceanogr.*, *35*, 474–488.

Ollitrault, M., M. Lankhorst, D. Fratantoni, P. Richardson, and W. Zenk (2006), Zonal intermediate currents in the equatorial Atlantic Ocean, *Geophys. Res. Lett.*, *33*, L05605, doi:10.1029/2005GL025368.

Oschlies, A., and V. Garcon (1999), An eddy-permitting coupled physical-biological model of the North Atlantic: 1. Sensitivity to advection numerics and mixed layer physics, *Global Biogeochem. Cycles*, *13*, 135–160.

Outdot, C., P. Morin, F. Baurand, M. Wafar, and P. Le Corre (1998), Northern and southern water masses in the equatorial Atlantic: Distributions of nutrients on the WOCE A6 and A7 lines, *Deep Sea Res., Part I*, *45*, 873–902.

Pacanowski, R. C. (1995), MOM 2 documentation, user's guide and reference manual, technical report, Ocean Group, Geophys. Fluid Dyn. Lab., Princeton, N. J.

Read, P. L., Y. H. Yamazaki, S. R. Lewis, P. D. Williams, K. Miki-Yamazaki, J. Sommeria, H. Didelle, and A. Fincham (2004), Jupiter's and Saturn's convectively driven banded jets in the laboratory, *Geophys. Res. Lett.*, *31*, L22701, doi:10.1029/2004GL020106.

Redi, M. H. (1982), Oceanic isopycnal mixing by coordinate rotation, *J. Phys. Oceanogr.*, *12*, 1154–1158.

Rhein, M., L. Stramma, and U. Send (1995), The Atlantic deep western boundary current: Water masses and transports near the equator, *J. Geophys. Res.*, *100*, 2441–2458.

Rhines, P. (1975), Waves and turbulence on a beta-plane, *J. Fluid Mech.*, *69*, 417–443.

Rhines, P. (1977), The dynamics of unsteady currents, in *The Sea*, vol. 6, edited by E. Goldberg, pp. 189–318, Wiley-Interscience, Hoboken, N. J.

Richards, K. J., N. A. Maximenko, F. O. Bryan, and H. Sasaki (2006), Zonal jets in the Pacific Ocean, *Geophys. Res. Lett.*, *33*, L03605, doi:10.1029/2005GL024645.

Robinson, W. A. (1997), Dissipation dependence of the jet latitude, *J. Clim.*, *10*, 176–182.

Sabine, C., et al. (2004), The oceanic sink for anthropogenic CO_2, *Science*, *305*, 367–371.

Schott, F. A., M. Dengler, P. Brandt, K. Affler, J. Fischer, B. Bourlès, Y. Gouriou, R. L. Molinari, and M. Rhein (2003), The zonal currents and transports at 35°W in the tropical Atlantic, *Geophys. Res. Lett.*, *30*(7), 1349, doi:10.1029/2002GL016849.

Stevens, D. P. (1990), On open boundary conditions for three dimensional primitive equation ocean circulation models, *Geophys. Astrophys. Fluid Dyn.*, *51*, 103–133.

Treguier, A. M., N. G. Hogg, M. Maltrud, K. Speer, and V. Thierry (2003), The origin of deep zonal flows in the Brazil Basin, *J. Phys. Oceanogr.*, *33*, 580–599.

Veronis, G. (1975), The role of models in tracer studies, in *Numerical Models of the Ocean Circulation*, pp. 133–146, Natl. Acad. of Sci., Washington, D. C.

Weiss, R., J. L. Bullister, R. H. Gammon, and M. J. Warner (1985), Atmospheric chlorofluoromethanes in the deep equatorial Atlantic, *Nature*, *314*, 608–610.

Wunsch, C., and R. Ferrari (2004), Vertical mixing, energy and the general circulation of the oceans, *Annu. Rev. Fluid Mech.*, *36*, 281–314.

C. Eden, IFM-GEOMAR, Düsternbrooker Weg 20, D-24105 Kiel, Germany. (ceden@ifm-geomar.de)